Modeling the aggregation of partially covered particles: Theory and simulation

A. Moncho-Jordá,[1,*] G. Odriozola,[2,†] M. Tirado-Miranda,[3,‡] A. Schmitt,[1,§] and R. Hidalgo-Álvarez[1,‖]

[1]*Departamento de Física Aplicada, Universidad de Granada, Campus Fuentenueva, E-18071 Granada, Spain*

[2]*Programa de Ingeniería Molecular, Instituto Mexicano del Petróleo, Lázaro Cárdenas 152, 07730 México, Distrito Federal, Mexico*

[3]*Departamento de Física, Escuela Politécnica, Universidad de Extremadura, Avenida de la Universidad, 10071 Cáceres, Spain*

(Received 2 February 2003; published 15 July 2003)

A theoretical model for describing the initial stages of the aggregation of partially covered colloidal particles is presented. It is based on the assumption of short-range interactions that may be modeled by a sticking probability on contact. Three types of sticking probabilities are distinguished depending on the collision type, i.e., for bare-bare, bare-covered, and covered-covered collisions. Hence, the model allows an analytical expression for the dimer-formation rate constant k_{11}, to be deduced as a function of the degree of surface coverage and the three sticking probabilities. The theoretical predictions are contrasted with simulated data. The observed agreement between theory and simulations shows the usefulness of the model for predicting the initial stages of this kind of aggregation processes.

DOI: 10.1103/PhysRevE.68.011404 PACS number(s): 61.43.Hv, 02.50.−r, 82.70.Dd, 05.40.Jc

I. INTRODUCTION

Macromolecules adsorbed onto colloidal particle surfaces may either stabilize or destabilize the dispersions. This makes the employment of macromolecules as additives for suspensions a much extended practice for industrial purposes. Several applications can be found in mineral and waste water treatments, such as water treatments for human consumption, paper industry, drilling fluids, ceramics, agrochemical formulation, and in immunoassay diagnostic test design [1]. However, such processes are so highly complex in nature that they have not been completely understood, yet.

Given any particular situation where macromolecules and colloidal particles are taking part, the process will depend on the degree of surface coverage with macromolecules and on the macromolecule-macromolecule and macromolecule-particle interactions [2,3]. When the particle surface is fully covered by the macromolecules, the observed result is generally a stabilized suspension [4,5]. For partially covered surfaces, however, the already adsorbed macromolecules on a given particle may attach to the bare patch of another one forming a particle-particle bridge (bridging flocculation) [6,7].

It is well known that the bridging flocculation rate depends on the degree of surface coverage. The classical work of La Mer and Healy [8] predicts a maximum of the flocculation rate when half the total surface is covered by macromolecules. When additional factors contribute to destabilization, the optimum degree of surface coverage usually becomes smaller [9].

In spite of the large amount of experimental work that has been performed for studying different aspects of these types of systems [10–18], there is still a lack of theoretical models for explaining their flocculation kinetics. In this work we attempt to fill this gap proposing a model based on La Mer's idea of a surface coverage dependent aggregation rate capable of describing the initial stages of an aggregation process. Additionally, the concepts of sticking probability and consecutive collisions recently employed for modeling the transition from diffusion to reaction limited cluster aggregation are also included [19,20]. The obtained results are then compared with Brownian dynamics simulations.

The paper is organized as follows. Section II reports the theoretical background. Section III briefly describes the simulations, presents some simulation results, and confirms that the models found in the literature are not capable of matching the data. In Sec. IV an alternative model is proposed and its predictions are compared with the simulated data. Finally, Sec. V tackles the conclusions.

II. THEORETICAL BACKGROUND

Colloidal aggregation processes may be monitored by the time evolution of the cluster concentrations, $c_i(t) = n_i(t)/V$, where $n_i(t)$ is defined as the number of clusters of size i at time t, and V is the whole volume where the aggregation takes place. For dilute systems the time evolution of the cluster concentrations is given by the Smoluchowski equation [21,22]:

$$\frac{dc_i}{dt} = \frac{1}{2}\sum_{j=1}^{i-1} k_{j,i-j}c_j(t)c_{i-j}(t) - c_i(t)\sum_{j=1}^{\infty} k_{ij}c_j(t). \quad (1)$$

The kinetic rate constants, or the aggregation kernel, k_{ij}, represent the mean rate at which two i- and j-size clusters stick to form a $(i+j)$-size cluster. It contains all physical information about the kinetics of the aggregating system. The cluster concentrations $c_i(t)$ are average quantities that do not consider the internal cluster structure. Nevertheless, this information is implicitly included in the size dependence of the kernel k_{ij}. It should be noted that the kernel is an orientational and morphological average of all particular cluster formation possibilities.

*Email address: moncho@ugr.es
†Email address: godriozo@imp.mx
‡Email address: mtirado@ugr.es
§Email address: schmitt@ugr.es
‖Email address: rhidalgo@ugr.es

Two irreversible aggregation regimes have been reported in the literature, diffusion limited cluster aggregation (DLCA) and reaction limited cluster aggregation (RLCA). Their differences lie basically in the strength of the particle-particle interactions on contact. For DLCA, the clusters diffuse in the absence of interparticle forces and, consequently, the motion is purely Brownian. A pair of clusters only interact on contact, when a short-range infinitely deep potential well holds them together and forces them to form a larger cluster. Afterwards, the newly formed cluster continues its free diffusive motion until it disappears when it collides with any other cluster. The DLCA regime is well described by the Brownian aggregation kernel

$$k_{ij}^{Br}=\frac{k_{11}^{Br}}{4}(i^{1/d_f}+j^{1/d_f})(i^{-1/d_f}+j^{-1/d_f}), \tag{2}$$

where d_f is the cluster fractal dimension. For DLCA processes, its value lies typically close to 1.75 when particle rearrangements within the clusters do not take place. DLCA is the fastest possible aggregation mode in the absence of attractive interactions. The corresponding Brownian dimer formation rate constant is given by [22]

$$k_{11}^{Br}=\frac{8k_BT}{3\eta_0}, \tag{3}$$

where k_B is the Boltzmann constant, T is the temperature, and η_0 is the solvent viscosity. For water at $T=293$ K, one obtains $k_{11}^{Br}=10.79\times10^{-18}$ m^3 s^{-1}.

An aggregation process becomes reaction controlled (RLCA) when, as a result of the repulsive interactions between the clusters, only a small fraction of collisions leads to aggregation. This corresponds to the presence of a short-range repulsive potential barrier, so that the number of effective collisions decreases as the barrier height grows. When the particle-particle interactions are sufficiently short ranged, both particles and clusters perform free Brownian motion and may be assumed to interact only when they collide. For this particular case, the influence of the repulsive barrier on the cluster aggregation may be understood through a sticking probability P defined as the fraction of effective collisions leading to the formation of new bonds [23,24]. Since, in general, more than one collision is needed for aggregation in this regime and taking into account that these collisions may take place between a given pair of clusters or may even involve several clusters, we distinguish between cluster-cluster collision and cluster-cluster *encounter*. The latter is defined as a sequence of consecutive collisions that a given pair of clusters perform. Hence, an encounter starts with a first collision and ends when aggregation takes place or when at least one of the involved clusters diffuses away to collide with others. Recently, the following kernel for the RLCA regime has been proposed by considering these concepts [19,20]:

$$k_{ij}=k_{ij}^{Br}\frac{P}{1-(1-P)(P_c)_{ij}}, \tag{4}$$

where $(P_c)_{ij}$ is defined as the probability for two i- and j-size clusters to collide again after a given noneffective collision. This probability is related to the average number of collisions per encounter for a nonaggregating system $\mathcal{N}_{ij}$ by

$$\mathcal{N}_{ij}=\frac{1}{1-(P_c)_{ij}}. \tag{5}$$

Since bigger clusters have a larger cross section, $\mathcal{N}_{ij}$ must be an increasing function of the cluster size. The kernel given by Eq. (4) accounts for both the effect of the sticking probability and the influence of multiple consecutive collisions that may occur during encounters.

When particles are partially covered by, for example, irreversibly adsorbed macromolecules (say polymers, proteins, etc.), the sticking probability for two colliding particles will depend on whether the colliding surface patches are covered or not [25]. Since covered and bare parts interact in a different way, three types of collisions can be distinguished.

(1) Type 1: Collisions between two bare (uncovered) parts of the surfaces, i.e., a typical collision between conventional colloidal particles. The corresponding sticking probability is denoted by α_1. It depends usually on the energy barrier that arises due to repulsive electric double layer interactions and attractive London–van der Waals-type forces.

(2) Type 2: Collisions between a covered part of a particle and a bare part of another one. In this case, α_2 represents the probability for a macromolecule bridge to be formed between the particle surfaces (bridging flocculation).

(3) Type 3: Collisions between two covered surface patches. In this case, the sticking probability α_3 parameterizes the influence of steric interactions due to the absorbed macromolecule layers. Since steric effects usually impede aggregation, the value of α_3 is generally quite low and so this kind of aggregation process is also known as weak flocculation.

The probability for finding a covered surface patch is given by the degree of surface coverage ϕ. Analogously, the probability of finding a bare patch is given by $(1-\phi)$. According to these definitions, the fractions of collisions that occur in configurations 1 and 3 are $(1-\phi)^2$ and ϕ^2, respectively. For collisions of type 2, i.e., a collision between a bare and a covered patch, the probability reads $\phi(1-\phi)+(1-\phi)\phi=2\phi(1-\phi)$. From now on, we will refer to this factors as geometrical probabilities.

In general, the complete set of rate constants k_{ij} is required to predict the time evolution of the cluster concentrations. However, since at the beginning of the aggregation process only monomers exist in the system, the initial stages are fully determined by the dimer-formation rate constant k_{11}. In this work, we will focus our attention on the calculation of this rate constant.

Multiplying the geometrical probabilities by the corresponding sticking probabilities and summing for the three possible configurations, the overall effective sticking probability becomes

$$P^0(\phi)=\alpha_1(1-\phi)^2+\alpha_2 2\phi(1-\phi)+\alpha_3\phi^2. \tag{6}$$

A very simple expression for k_{11} immediately follows as

$$k_{11}(\phi) = k_{11}^{Br} P^0(\phi), \tag{7}$$

which already includes the well-known La Mer [8,26], Moudgil [27] and Molski [28] ideas. Equation (7), however, does not account for the possibility of two reacting monomers to collide several times during an encounter. Hence, a more appropriate expression for k_{11} should be deduced. This may be done by starting from Eq. (4), which already accounts for multiple monomer-monomer collisions during encounters. Doing so, one obtains

$$k_{11}(\phi) = k_{11}^{Br} \frac{P^0(\phi)}{1-[1-P^0(\phi)]P_c}. \tag{8}$$

Here, $P_c \equiv (P_c)_{11}$ denotes the probability for two monomers to collide again after a non-effective collision. The aggregation kernels given by Eqs. (7) and (8) express the dimer-formation rate constant as a function of the degree of surface coverage and the sticking probabilities, and so both of them may be employed to describe the aggregation process of partially covered particles.

III. SIMULATIONS

The aggregation processes were simulated off lattice and periodic boundary conditions were considered. Initially, $N_0 = 25\,000$ spherical particles of radius unity were randomly scattered in a cube box of side L, avoiding particle overlap. The box side was fixed to $L = 1015$ in order to obtain a volume fraction of $\psi_v = 0.0001$. The simulations were performed as explained in Refs. [29,30]. These types of simulations relate the average diffusion coefficient of an i-size cluster D_i to the cluster radius of gyration R_g through the Stokes law. The fractal nature of the clusters is accounted by $D_i \sim 1/R_g \sim i^{-1/d_f}$. The simulations do not account for the Brownian rotation of single particles or clusters.

In order to describe the aggregation of partially covered particles, the original simulation algorithm has to be extended for considering a certain fraction of the particle surface to be covered by macromolecules. Furthermore, the three possible types of cluster-cluster collisions (bare-bare, bare-covered, and covered-covered) must be distinguished and their corresponding sticking probabilities (α_1, α_2, and α_3) must be taken into account. Hence, when a cluster-cluster collision occurs, the collision type is determined and the sticking probability is set accordingly.

It should be pointed out that the spatial distribution of macromolecules adsorbed on the particles' surfaces is generally not known for real experimental systems. The coverage may be scattered homogeneously over the whole particle surface, or concentrated in a single spot, or even dispersed in several smaller spots. The homogeneous case, where all collisions have the same sticking probability, corresponds to the well-known RLCA regime. For a single adsorbed spot, however, the particle orientation plays a crucial role for aggregation and the dimer-formation rate constant is expected to depend very strongly on the spot size, i.e., the fractional surface coverage ϕ. In this work, we will focus our attention on this extreme case. It would also be quite interesting to study the transition from the single spot case to the homogeneous one, although this is beyond the scope of this work.

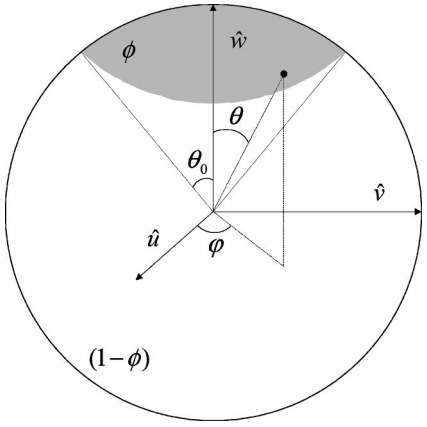

FIG. 1. A spherical particle covered partially by a single spherical spot (gray zone). The angular size and the orientation vector of the spot are given by θ_0 and $\hat{w}$, respectively.

Figure 1 shows a spherical particle partially covered by a single spherical spot. The size and orientation of the spot are given by the aperture angle θ_0 and the orientation vector $\hat{w}$, respectively. The unitary orientation vector $\hat{w}$, pointing from the particle center to the center of the surface spot, is randomly chosen for each particle at the beginning of the simulation. Since we do not allow for rotational particle diffusion, this vector remains unaltered during the whole aggregation process and, consequently, may be considered as an intrinsic property of the particles.

The degree of surface coverage ϕ is related to the angular spot size θ_0 by

$$\phi \equiv \frac{1}{4\pi}\int_0^{2\pi} d\varphi \int_0^{\theta_0} \sin\theta \, d\theta = \frac{1}{2}(1-\cos\theta_0). \tag{9}$$

In order to determine which of the three possible configurations for a pair of particles A and B on contact is occurring, the following test is made: if $\hat{w}_A \cdot \hat{r}_{AB} \geqslant \cos\theta_0 = (1-2\phi)$, then particle A collides in its covered part. On the contrary, if $\hat{w}_A \cdot \hat{r}_{AB} < (1-2\phi)$, then the bare part of particle A is involved. Performing the same test for particle B the collision type is determined (Fig. 2).

The dimer-formation rate constant is easily obtained from the temporal evolution of the monomer concentration $c_1(t) = n_1(t)/V$ for short aggregation times. For the initial stages of the aggregation process, $c_1(t)$ may be calculated assuming a constant kernel solution of the Smoluchowski equation, $k_{ij} = k_{11} = k_s$ [31],

$$g(t) \equiv \frac{2V}{N_0}\left[\sqrt{\frac{N_0}{n_1(t)}} - 1\right] = k_{11} t. \tag{10}$$

Plotting the left-hand side of the above equation as a function of the aggregation time and fitting a straight line allows us to obtain k_{11} as the slope of the fitted curve by considering the known initial monomer concentration $c_1(0) = N_0/V$. Al-

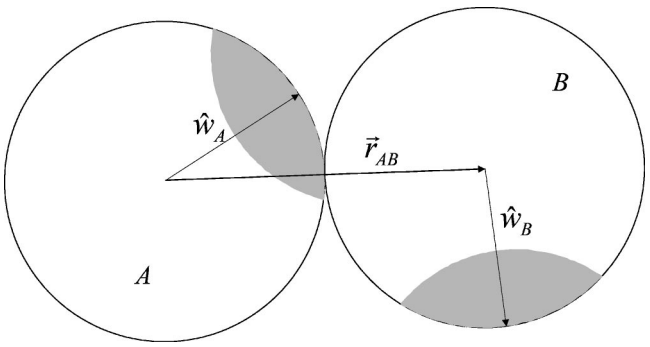

FIG. 2. Schematic view of a typical collision between two spherical, partially covered, particles. $\hat{w}_A$ and $\hat{w}_B$ are the unitary vectors pointing to the spot centers, and $\hat{r}_{AB}=\frac{1}{2}\vec{r}_{AB}$ represents a unitary vector joining the centers of the particles when contact is stablished.

though the validity of Eq. (10) is restricted to short times, this approximation leads to accurate k_{11} values.

Figure 3 shows a typical time evolution of $g(t)$ (solid line) and the corresponding short-time linear fit (dashed line). As can be seen, $g(t)$ is well described by a straight line along a broad enough time interval.

Simulation results

The k_{11}^{Br} value obtained by means of computer simulations for the DLCA regime ($\alpha_1=\alpha_2=\alpha_3=1$) is $k_{11}^{Br}=(10.83\pm0.04)\times10^{-18}$ m^3 s^{-1}. This value is in good agreement with the theoretical prediction given by Eq. (3). We also computed the average number of monomer-monomer collisions per encounter in a nonaggregating system ($P=0$), since this parameter is required for Eq. (8). The result is $\mathcal{N}_{11}=6.154$, which leads to $P_c=(P_c)_{11}=0.8375$.

In order to study the effect of the surface coverage, six groups of simulations were performed differing only in their respective sticking probabilities (see Table I).

For real experiments group III may represent the aggregation of partially covered particles by macromolecules, where collisions between two covered parts are forbidden due to steric repulsive interactions, whereas bridging flocculation and normal coagulation are always accepted. Similarly, group V represents pure bridging flocculation, where aggregation occurs only between covered and uncovered patches of the colliding particles. On the contrary, group VI may describe a dimerization reaction between anisotropic species having only one active site each. This kind of reaction is very frequent at molecular level. These six groups are the simplest cases we may study. Although sticking probabilities distinct from 0 or 1 are expected to be obtained in many kinds of real experiments, these six groups represent an appropriate starting point for our study and allow for a first approach to the different underlying aggregation mechanisms.

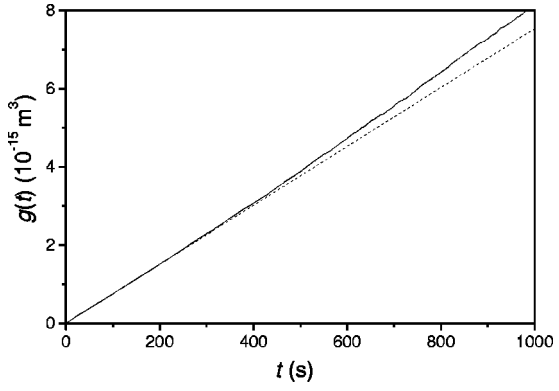

FIG. 3. Time evolution of $g(t)=(2V/N_0)[\sqrt{N_0/n_1(t)}-1]$ obtained for a typical simulation (solid line) and the corresponding short-time linear fit (dashed line).

TABLE I. Sticking probabilities for the six groups considered for the simulations.

	I	II	III	IV	V	VI
α_1	0	1	1	1	0	0
α_2	1	0	1	0	1	0
α_3	1	1	0	0	0	1

The obtained results are summarized in Fig. 4. There, the relative rate constant $k_{11}^{rel}=k_{11}/k_{11}^{Br}$ is plotted as a function of ϕ for the six groups of sticking probabilities (square symbols). For group I, k_{11}^{rel} increases monotonically from 0 to 1. On the contrary, for group III a monotonic decrease is observed. For group II the initial aggregation rate goes from the DLCA value at $\phi=\{0,1\}$ to its minimum value at $\phi=0.5$, where $k_{11}^{rel}=0.708$. For group IV, a monotonic decay of k_{11}^{rel} from the DLCA limit to 0 is also observed, just like the behavior obtained for group III. The decrease, however, is faster since aggregation for covered-bare patches is forbidden ($\alpha_2=0$). For group VI, the initial aggregation rate grows from 0 to the DLCA value, although the increase is slower than the observed for group I (also due to the fact of having $\alpha_2=0$). Finally, in group V, coagulation is completely forbidden for $\phi=0$ and $\phi=1$, whereas the initial aggregation rate reaches its maximum value $k_{11}^{rel}=0.708$ at $\phi=0.5$.

It should be noted that, as expected, the simulation results show some symmetries among them. Indeed, groups III and VI turn into groups I and IV, respectively, by replacing ϕ by $(1-\phi)$. Also the curves corresponding to groups II and V are symmetric with respect to $\phi=0.5$.

Figure 4 also shows the theoretical predictions given by Eqs. (7) and (8) (dashed and solid lines, respectively). As can be observed, Eq. (7) underestimates the simulation results in all cases. This was an expected result since this model does not consider the possibility of several consecutive collisions per encounter that enhance aggregation. However, when the correction for multiple collisions is included in the kernel [Eq. (8)], the obtained theoretical curves by far overestimate the simulated data, i.e., particles are predicted to aggregate too fast.

Now, the following question arises from these observations: Why is expression (8) not capable to predict the simulation data? The problem is that, even though the effect of

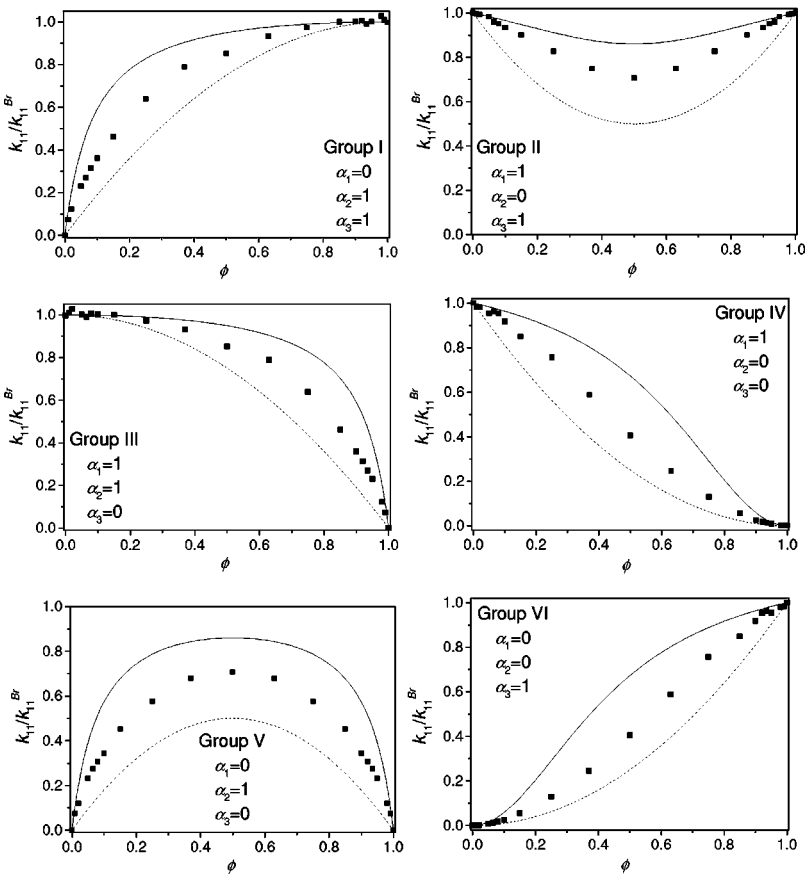

FIG. 4. The relative rate constant $k_{11}^{rel}=k_{11}/k_{11}^{Br}$ as a function of the degree of surface coverage ϕ obtained from the simulations for the six groups shown in Table I (square symbols). The dashed and solid lines are the theoretical predictions of Eqs. (7) and (8), respectively.

multiple collisions is considered, the model on which Eq. (8) is based assumes all consecutive collisions of a single encounter to be independent; that is, it takes the sticking probabilities to be P^0 for all types of collisions [see Eq. (6)]. However, it is clear that after a first collision, particles are oriented in a particular direction such that the effective sticking probability for the subsequent collisions will be, in general, different from P^0. In other words, after a monomer-monomer collision of certain type, there is a larger probability that the subsequent collisions turn to be of the same type. Hence, the previous model needs to be extended in order to account for the fact that the sticking probabilities are conditioned to the preceding type of collision. This will be done in the following section.

IV. THE PROPOSED MODEL AND ITS DISCUSSION

In order to achieve a good theoretical description of the simulation results, it is necessary to consider that the geometrical probabilities are conditioned to the previous collision type. For the purpose of simplifying the mathematical expressions, the notation introduced in Sec. II is employed, which identifies the bare-bare, bare-covered, and covered-covered collisions through the subindexes 1, 2, and 3, respectively. In the same way, we define P_{mn} as the conditional geometrical probability for a collision of type n occurring after a collision of type m for a given pair of particles. Hence, P_{12} represents the geometrical probability for a pair of particles to produce a bare-covered collision after a bare-bare collision. Notwithstanding, the geometrical probabilities are not conditioned for the first collision of any encounter. They are noted as P_{0n} for a n-type collision. Due to the normalization of the geometrical probabilities, the values of P_{mn} and P_{0n} are related by

$$\sum_{n=1}^{3} P_{mn}=1 \quad \forall\ m=1,2,3, \quad \sum_{n=1}^{3} P_{0n}=1. \tag{11}$$

Since for a first collision of an encounter the patches of both monomers are randomly oriented, we have

$$\begin{aligned} P_{01}(\phi)&=(1-\phi)^2,\\ P_{02}(\phi)&=2\phi(1-\phi),\\ P_{03}(\phi)&=\phi^2. \end{aligned} \tag{12}$$

It should by mentioned that the ϕ dependence of the geometrical probability matrix $\{P_{mn}(\phi)\}_{m,n=1-3}$ is unknown *a priori* and some realistic model is required. By the moment, however, we will develop the kinetic model, assuming that these quantities are already known. At the end of this section, we will return to this point in order to attempt for a reasonable approximation for this matrix.

In addition to the geometrical probabilities, the dimer-formation rate constant also depends on the sticking probabilities α_1, α_2, and α_3. Moreover, the probability for two monomers to collide again (P_c), the probability for two monomers to stop colliding and diffuse away ($1-P_c$), the average time between two consecutive collisions (t_c), and

the average diffusion time between two consecutive encounters (t_{dif}) must also be involved in the k_{11} expression.

The procedure for calculating k_{11} begins with the following identity:

$$k_{11}=\frac{V}{\langle t\rangle}, \tag{13}$$

where V is the volume of the whole system and $\langle t\rangle$ is the average lifetime of monomers [19,20]. If the sticking probabilities for the different types of collisions are the unity, $\alpha_1=\alpha_2=\alpha_3=1$, this lifetime becomes the average diffusion time, and the aggregation is described by the DLCA regime and the Brownian kernel

$$k_{11}^{Br}=\frac{V}{t_{dif}}. \tag{14}$$

The procedure for determining the average time $\langle t\rangle$ consists of considering all possible event times weighted with their corresponding probabilities. As an example, let us consider the following event: ''A pair of monomers diffuse, meet, and collide two times, being both collisions of type 1. Afterwards, the monomers diffuse away and one of them collides with a third monomer twice, being the first collision of type 3 and the second of type 2. During the last collision the monomers aggregate and form a dimer.'' The average time involved in this event is $t_{ev}=2t_c+2t_{dif}$ and the corresponding probability for it is $P_{ev}=P_{01}(1-\alpha_1)P_cP_{11}(1-\alpha_1)(1-P_c)P_{03}(1-\alpha_3)P_cP_{32}\alpha_2$. Figure 5 shows a tree diagram for the possible ways that this kind of aggregation process may follow considering up to three collisions. Defining the effective sticking probabilities P^0, P^1, P^2, and P^3 as

$$P^n(\phi)=\alpha_1P_{n1}+\alpha_2P_{n2}+\alpha_3P_{n3}, \quad n=0,1,2,3, \tag{15}$$

the average monomer lifetime may be expressed by the following expansion:

$$\begin{aligned}\langle t\rangle\equiv&\sum_{ev}P_{ev}t_{ev}\\ &=t_{dif}P^0+(t_{dif}+t_c)P_c\sum_{n=1}^{3}P_{0n}(1-\alpha_n)P^n+2t_{dif}\\ &\times(1-P_c)\sum_{n=1}^{3}P_{0n}(1-\alpha_n)P^0+(t_{dif}+2t_c)\\ &\times(P_c)^2\sum_{n,m=1}^{3}P_{0n}(1-\alpha_n)P_{nm}(1-\alpha_m)P^m\\ &+(2t_{dif}+t_c)P_c(1-P_c)\sum_{n,m=1}^{3}P_{0n}(1-\alpha_n)\\ &\times[P_{nm}(1-\alpha_m)P^0+P_{0m}(1-\alpha_m)P^m]+3t_{dif}(1-P_c)^2\\ &\times\sum_{n,m=1}^{3}P_{0n}(1-\alpha_n)P_{0m}(1-\alpha_m)P^0.\end{aligned} \tag{16}$$

For the further analysis, it is convenient to group the geometrical and the equivalent probabilities and express them in the following matrix forms:

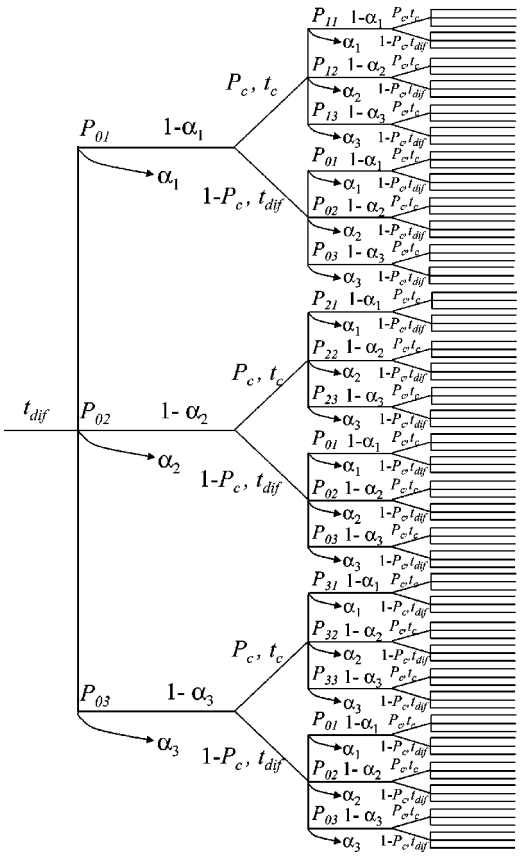

FIG. 5. Tree diagram for the possible ways that an aggregation process may follow considering up to three collisions. The corresponding probabilities and the involved average times are included. The average lifetime $\langle t\rangle$ is the sum of all event times weighted by their corresponding probabilities.

$$\vec{P}=(P^1,P^2,P^3), \tag{17}$$

$$\vec{P}^0=(P^0,P^0,P^0),$$

$$\vec{Q}^0=(Q_{01},Q_{02},Q_{03}),$$

$$\mathcal{A}=\begin{pmatrix}Q_{11}&Q_{12}&Q_{13}\\Q_{21}&Q_{22}&Q_{23}\\Q_{31}&Q_{32}&Q_{33}\end{pmatrix},$$

$$\mathcal{A}^0=\begin{pmatrix}Q_{01}&Q_{02}&Q_{03}\\Q_{01}&Q_{02}&Q_{03}\\Q_{01}&Q_{02}&Q_{03}\end{pmatrix},$$

where $Q_{0n}(\phi)\equiv P_{0n}(\phi)(1-\alpha_n)$ and $Q_{mn}(\phi)\equiv P_{mn}(\phi)(1-\alpha_n)$. Both, Q_{0n} and Q_{mn} contain all the mathematical dependence on the sticking probabilities and on the degree of coverage.

In terms of the above defined matrices, the average time turns

$$\langle t\rangle = t_{dif}P^0 + (t_{dif}+t_c)P_c\vec{Q}^0\cdot\vec{P} + 2t_{dif}(1-P_c)\vec{Q}^0\cdot\vec{P}^0 + (t_{dif}+2t_c)(P_c)^2\vec{Q}^0\cdot\mathcal{A}\cdot\vec{P} + (2t_{dif}+t_c)P_c(1-P_c) \times[\vec{Q}^0\cdot\mathcal{A}\cdot\vec{P}^0 + \vec{Q}^0\cdot\mathcal{A}^0\cdot\vec{P}] + 3t_{dif}(1-P_c)^2\vec{Q}^0\cdot\mathcal{A}^0\cdot\vec{P}^0 + \cdots . \quad (18)$$

However, instead of $\langle t\rangle$ it is convenient to calculate $\langle e^{xt}\rangle$. Hence,

$$\langle e^{xt}\rangle \equiv \sum_{ev} P_{ev}e^{xt_{ev}} = e^{xt_{dif}}P^0 + (e^{xt_{dif}}e^{xt_c})P_c\vec{Q}^0\cdot\vec{P} + e^{2xt_{dif}}(1-P_c)\vec{Q}^0\cdot\vec{P}^0 + (e^{xt_{dif}}e^{2xt_c})(P_c)^2\vec{Q}^0\cdot\mathcal{A}\cdot\vec{P} + (e^{2xt_{dif}}e^{xt_c})P_c(1-P_c)[\vec{Q}^0\cdot\mathcal{A}\cdot\vec{P}^0 + \vec{Q}^0\cdot\mathcal{A}^0\cdot\vec{P}] + e^{3xt_{dif}}(1-P_c)^2\vec{Q}^0\cdot\mathcal{A}^0\cdot\vec{P}^0 + \cdots . \quad (19)$$

The last sum may be written in the following form:

$$\langle e^{xt}\rangle = e^{xt_{dif}}P^0 + e^{xt_{dif}}\vec{Q}^0\cdot\{\mathcal{I} + [P_c\mathcal{A}e^{xt_c} + (1-P_c)\mathcal{A}^0e^{xt_{dif}}] + [P_c\mathcal{A}e^{xt_c} + (1-P_c)\mathcal{A}^0e^{xt_{dif}}]^2 + \cdots\}\cdot[P_ce^{xt_c}\vec{P} + (1-P_c)e^{xt_{dif}}\vec{P}^0], \quad (20)$$

where $\mathcal{I}$ is the 3×3 identity matrix. We define the matrix $\mathcal{H}$ as

$$\mathcal{H}(x) \equiv \sum_{n=0}^{\infty}[P_c\mathcal{A}e^{xt_c} + (1-P_c)\mathcal{A}^0e^{xt_{dif}}]^n = [\mathcal{I} - P_c\mathcal{A}e^{xt_c} - (1-P_c)\mathcal{A}^0e^{xt_{dif}}]^{-1}. \quad (21)$$

Here, $\mathcal{U}^{-1}$ represents the inverse matrix of $\mathcal{U}$. Using Eq. (21) in Eq. (20), we finally obtain the following expression that contains the contributions for all possible events

$$\langle e^{xt}\rangle = e^{xt_{dif}}\{P^0 + \vec{Q}^0\cdot\mathcal{H}(x)\cdot[P_ce^{xt_c}\vec{P} + (1-P_c)e^{xt_{dif}}\vec{P}^0]\}. \quad (22)$$

The exact mathematical expression for the average monomer lifetime may be obtained from the above equation by means of the relationship

$$\langle t\rangle = \left(\frac{\partial\langle e^{xt}\rangle}{\partial x}\right)_{x=0}. \quad (23)$$

It becomes

$$\langle t\rangle = t_{dif}P^0 + \vec{Q}^0\cdot\left(\frac{d\mathcal{H}}{dx}\right)_{x=0}\cdot[P_c\vec{P} + (1-P_c)\vec{P}^0] + \vec{Q}^0\cdot\mathcal{H}(0)\cdot[(t_{dif}+t_c)P_c\vec{P} + 2t_{dif}(1-P_c)\vec{P}^0]. \quad (24)$$

The average time between two consecutive monomer-monomer collisions, t_c, is much shorter than the average diffusion time. In fact, for the simulation conditions given in Sec. III we obtained $t_c/t_{dif} = 3.96\times10^{-3}$. Hence, we may safely assume $t_c \approx 0$ in order to simplify Eq. (24). By doing so, the kinetic rate constant k_{11} may be obtained by only replacing this average lifetime on Eqs. (13) and (14) while considering expressions (17) and (21). Its final explicit form is given by

$$\frac{k_{11}}{k_{11}^{Br}} = 1-(1-P_c)\frac{B_U + C_UP_c + D_U(P_c)^2}{1 - C_DP_c - D_D(P_c)^2 - E_D(P_c)^3}, \quad (25)$$

where

$$B_U = Q_{01} + Q_{02} + Q_{03}, \quad (26)$$

$$C_U = Q_{01}(Q_{12}+Q_{13}-Q_{22}-Q_{33}) + Q_{02}(Q_{21}+Q_{23}-Q_{11}-Q_{33}) + Q_{03}(Q_{31}+Q_{32}-Q_{11}-Q_{22}),$$

$$D_U = Q_{01}(Q_{12}Q_{23}+Q_{13}Q_{32}+Q_{22}Q_{33}) - Q_{01}(Q_{12}Q_{33}+Q_{13}Q_{22}+Q_{23}Q_{32}) + Q_{02}(Q_{23}Q_{31}+Q_{21}Q_{13}+Q_{11}Q_{33}) - Q_{02}(Q_{21}Q_{33}+Q_{23}Q_{11}+Q_{13}Q_{31}) + Q_{03}(Q_{31}Q_{12}+Q_{32}Q_{21}+Q_{11}Q_{22}) - Q_{03}(Q_{31}Q_{22}+Q_{32}Q_{11}+Q_{12}Q_{21}),$$

$$C_D = Q_{11}+Q_{22}+Q_{33},$$

$$D_D = Q_{12}Q_{21}+Q_{13}Q_{31}+Q_{23}Q_{32} - (Q_{11}Q_{22}+Q_{11}Q_{33}+Q_{22}Q_{33}),$$

$$E_D = \det\mathcal{A}.$$

Note that this expression has the form $k_{11}/k_{11}^{Br} = 1-\Delta(\phi)$, where $\Delta(\phi)$ is a positive quantity which represents the correction to the Brownian kernel due to noneffective collisions. The above expression gives us the dimer-formation rate constant whatever the values of the sticking probabilities are, for the three possible types of collisions and for all possible degrees of surface coverage, $k_{11} = k_{11}(\alpha_1,\alpha_2,\alpha_3,\phi)$. Therefore, it completely describes the initial stages of the aggregating system. Moreover, Eq. (25) has a general validity, i.e., it does not depend on the way in which the surface coverage is distributed on the particle surface. In other words, it can be applied when the surface coverage is concentrated in a single circular spot or even when it is scattered over the surface in several smaller spots. The only difference between these two cases lies on the expressions for the conditional geometrical probabilities, P_{mn}.

The general form, given by Eq. (25), may be simplified when some specific situations are considered. In the following section, we discuss the simplest ones.

A. Particular cases

(1) All types of collisions have the same sticking probability: $\alpha_1=\alpha_2=\alpha_3=\alpha$. Then, considering the normalization condition [Eq. (11)] we have $P^0=P^1=P^2=P^3=\alpha$, $Q_{0n}=P_{0n}(1-\alpha)$ and $Q_{mn}=P_{mn}(1-\alpha)$. Using these relations in Eqs. (25) and (26) we obtain

$$\frac{k_{11}}{k_{11}^{Br}}=\frac{\alpha}{1-(1-\alpha)P_c}. \tag{27}$$

Since all types of collisions have the same sticking probability, the aggregation rate does not depend on the geometrical probabilities and on the degree of coverage. Therefore, the dimer-formation rate constant becomes simplified to the original expression for RLCA with $P=\alpha$ [see Eq. (4) for $i=j=1$].

(2) The geometrical probability for all types of collisions is always at random and it does not depend on the previous one. In this case $P_{mn}=P_{0n}$ and $\mathcal{A}=\mathcal{A}^0$. This leads to

$$\frac{k_{11}}{k_{11}^{Br}}=\frac{P^0}{1-(1-P^0)P_c}, \tag{28}$$

where $P^0=\alpha_1P_{01}+\alpha_2P_{02}+\alpha_3P_{03}$. Again, the classical RLCA form is obtained having an effective sticking probability $P=P^0$ [see Eq. (8)].

(3) Aggregation is forbidden for collisions of type n and it is always accepted for the other types: $\alpha_m=1-\delta_{mn}$. Now, $Q_{0m}=P_{0m}\delta_{mn}$ and $Q_{rm}=P_{rm}\delta_{mn}$ and, using $k_{11}/k_{11}^{Br}=1-\Delta$, one obtains for the correction Δ,

$$\Delta_{\alpha_1=0}^{\alpha_2,\alpha_3=1}=(1-P_c)\frac{P_{01}}{1-P_cP_{11}},$$

$$\Delta_{\alpha_2=0}^{\alpha_1,\alpha_3=1}=(1-P_c)\frac{P_{02}}{1-P_cP_{22}}, \tag{29}$$

$$\Delta_{\alpha_3=0}^{\alpha_1,\alpha_2=1}=(1-P_c)\frac{P_{03}}{1-P_cP_{33}}.$$

(4) Coagulation is always accepted for collisions of type n and it is forbidden for the other types: $\alpha_m=\delta_{mn}$. In this case, $Q_{0m}=P_{0m}(1-\delta_{mn})$ and $Q_{rm}=P_{rm}(1-\delta_{mn})$ and the Δ expression is given by

$$\Delta_{\alpha_1=1}^{\alpha_2,\alpha_3=0}=(1-P_c)\frac{P_{02}[1-P_c(P_{33}-P_{23})]+P_{03}[1-P_c(P_{22}-P_{32})]}{(P_{22}+P_{33})P_c+(P_{22}P_{33}-P_{23}P_{32})(P_c)^2},$$

$$\Delta_{\alpha_2=1}^{\alpha_1,\alpha_3=0}=(1-P_c)\frac{P_{01}[1-P_c(P_{33}-P_{13})]+P_{03}[1-P_c(P_{11}-P_{31})]}{1-(P_{11}+P_{33})P_c+(P_{11}P_{33}-P_{13}P_{31})(P_c)^2},$$

$$\Delta_{\alpha_3=1}^{\alpha_1,\alpha_2=0}=(1-P_c)\frac{P_{01}[1-P_c(P_{22}-P_{12})]+P_{02}[1-P_c(P_{11}-P_{21})]}{1-(P_{11}+P_{22})P_c+(P_{11}P_{22}-P_{12}P_{21})(P_c)^2}. \tag{30}$$

Note that Δ depends on the degree of surface coverage ϕ through the geometrical probabilities P_{mn} in expressions (28)–(30).

B. The geometrical probabilities P_{mn}

As mentioned before, the geometrical probabilities are well described by expression (12) for the first collision of any encounter. For the subsequent consecutive collisions, however, the situation is not as simple. As was previously shown, to assume all geometrical probabilities to be history independent leads to an overestimation of the aggregation rate. Hence, it becomes a necessity to account for the particle orientation during the previous collision.

The nine conditional geometrical probabilities are connected among them through the normalization condition [Eq. (11)]. Hence, only six probabilities are really independent. Furthermore, there exist the following symmetries:

$$\begin{aligned}
P_{11}(\phi)&=P_{33}(1-\phi),\\
P_{22}(\phi)&=P_{22}(1-\phi),\\
P_{13}(\phi)&=P_{31}(1-\phi),\\
P_{12}(\phi)&=P_{32}(1-\phi),\\
P_{21}(\phi)&=P_{23}(1-\phi).
\end{aligned} \tag{31}$$

Consequently, we have to obtain an expression for the conditional geometrical probabilities, P_{mn}, that is compatible with the normalization condition and with the symmetry relationships [expressions (11) and (31)].

For the sake of simplicity, we denote $\phi_c=\phi$ and $\phi_b=(1-\phi)$ as the fractions of covered and bare surface, respectively, such that $\phi_c+\phi_b=1$. Let us suppose that the first collision between a pair of particles is of type 3, i.e., it involves a covered-covered contact [see Fig. 6(a)]. Since the

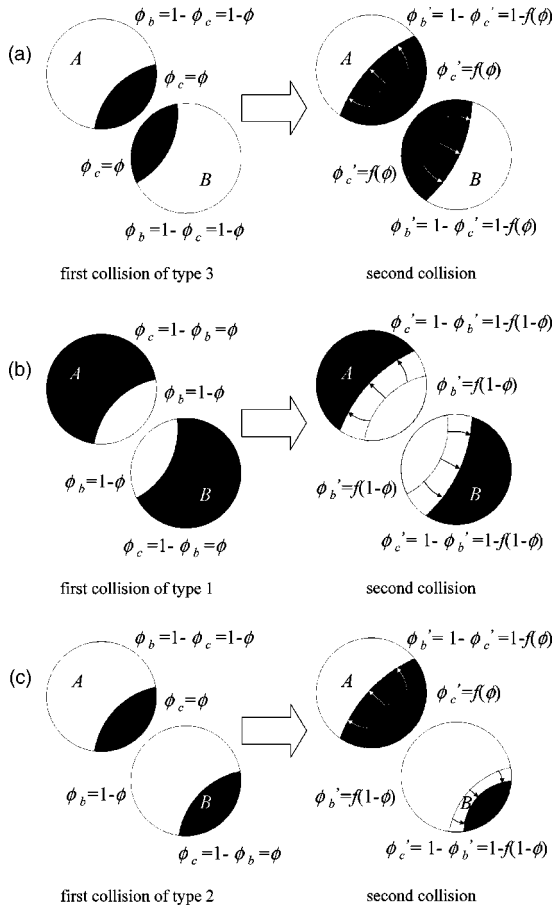

FIG. 6. Schematic view of the three possible situations that may appear as a consequence of a first collision. Situation (a) is obtained after the first collision of type 3, (b) is the result of a collision of type 1, and (c) is that of type 2. In all cases, $\phi_c=\phi$ and $\phi_b=(1-\phi)$ denote the fractions of covered and uncovered surface, respectively. Function $f(\phi_c)$ $[f(\phi_b)]$ represents the value of the localized ϕ_c $[\phi_b]$ around the contact point. That is, function f gives us the probability of finding a given surface patch again after a collision on this patch (see text).

first collision occurs at random orientation, the geometrical probabilities are given by $P_{01}=\phi_b\phi_b=(1-\phi)^2$, $P_{02}=2\phi_b\phi_c=2\phi(1-\phi)$, and $P_{03}=\phi_c\phi_c=\phi^2$. Afterwards, both particles are oriented in a particular direction and they can explore only a relative small part of their respective surfaces. Consequently, the conditional geometrical probabilities P_{31}, P_{32}, and P_{33} will, in general, differ from the product of the fraction of covered and bare surfaces, ϕ_c and ϕ_b, respectively.

It seems convenient to define an effective surface coverage $\phi_c'=f(\phi_c)=f(\phi)$ and $\phi_b'=1-\phi_c'=1-f(\phi)$ such that the former product expressions remain valid. Here, ϕ_c' (ϕ_b') represents the value of the localized ϕ_c (ϕ_b) around the contact point. In other words, we treat the second collision as if it had occurred between two randomly oriented particles with a *renormalized* effective surface coverage, ϕ_b' and ϕ_c'. Hence, $P_{31}=\phi_b'\phi_b'=[1-f(\phi)]^2$, $P_{32}=2\phi_b'\phi_c'=2f(\phi)[1-f(\phi)]$, and $P_{33}=\phi_c'\phi_c'=f(\phi)^2$. These concepts are schematically represented in Fig. 6 for all possible types of collisions. It also shows that the surface spot where the particles collided the first time looks larger in the subsequent collision (see arrows). The general expressions for the conditional geometrical probabilities read as follows:

$$P_{11}=\phi_b'\phi_b'=f(1-\phi)^2,$$

$$P_{12}=2\phi_b'(1-\phi_b')=2f(1-\phi)[1-f(1-\phi)],$$

$$P_{13}=(1-\phi_b')(1-\phi_b')=[1-f(1-\phi)]^2,$$

$$P_{21}=(1-\phi_c')\phi_b'=[1-f(\phi)]f(1-\phi),$$

$$\begin{aligned}P_{22}&=\phi_c'\phi_b'+[1-\phi_c'][1-\phi_b']\\&=f(\phi)f(1-\phi)+[1-f(\phi)][1-f(1-\phi)],\end{aligned}\quad(32)$$

$$P_{23}=\phi_c'(1-\phi_b')=f(\phi)[1-f(1-\phi)],$$

$$P_{31}=(1-\phi_c')(1-\phi_c')=[1-f(\phi)]^2,$$

$$P_{32}=2\phi_c'(1-\phi_c')=2f(\phi)[1-f(\phi)],$$

$$P_{33}=\phi_c'\phi_c'=f(\phi)^2.$$

The above expressions verify both the normalization condition [Eq. (11)] and the symmetry relationships [Eq. (31)] in a natural way. Since ϕ represents the probability of finding a covered surface part for a first collision, $f(\phi)$ denotes the probability for finding a covered surface patch after a collision on the covered part. It should be noted that only the function $f(\phi)$ is necessary in order to know all the geometrical probabilities. The explicit form of function f will be determined by comparing the theoretical predictions with simulation results. Since the geometrical probabilities do not depend on the sticking probabilities α_1, α_2, and α_3, we can use the simplest simulation conditions for deducing $f(\phi)$.

C. Discussion

The relative kinetic rate constants, obtained by means of simulations for the six groups mentioned in Table I, have been fitted theoretically using $k_{11}^{rel}=1-\Delta$. Groups I, II, and III correspond to the particular case (3), specifically to the three equations shown in Eqs. (29), respectively. Analogously, groups IV, V, and VI are theoretically described by the particular case (4) through Eqs. (30).

In these expressions, the sticking probabilities α_1, α_2, and α_3 together with the degree of surface coverage ϕ are input parameters given by the simulation conditions. Also $P_c=0.8375$ is kept constant for all cases. Consequently, the only free parameter is the unknown function $f(\phi)$. Therefore, the following empiric expression is proposed for $f(\phi)$:

$$f(\phi)=\phi^{\mu-4\nu\phi(1-\phi)}.\quad(33)$$

Here, μ and ν are two fitting parameters that do not depend on ϕ. On the one hand, $\mu-\nu$ controls the value of k_{11}^{rel} at

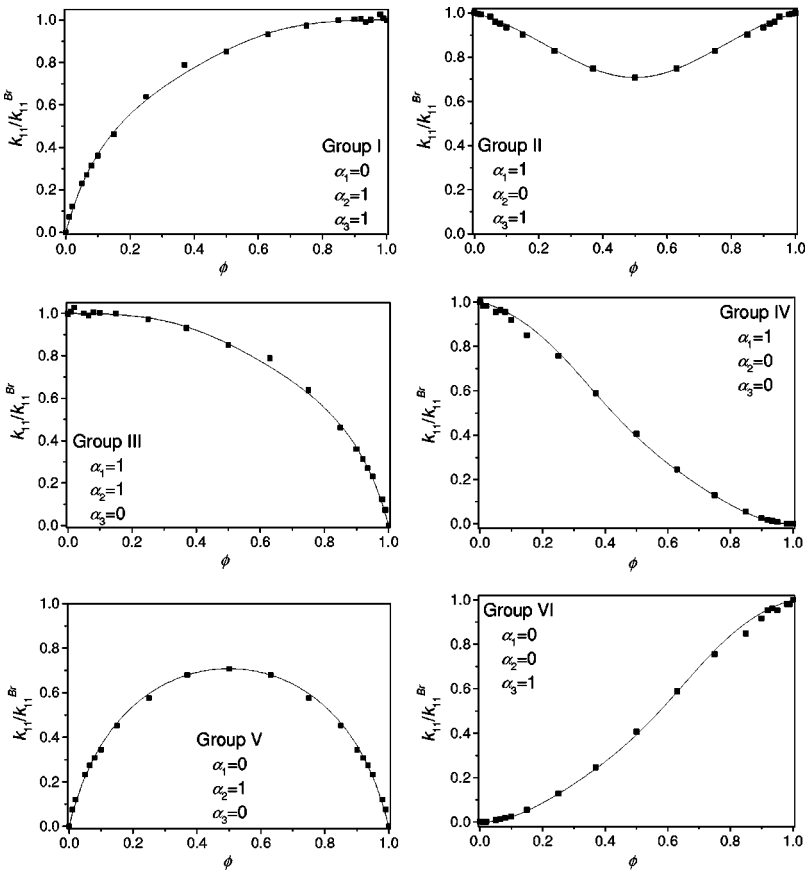

FIG. 7. The same simulated $k_{11}^{rel}=k_{11}/k_{11}^{Br}$ data shown in Fig. 4 (square symbols) are compared to the theoretical predictions obtained by using the kinetic model given by Eq. (25) (solid lines). The curves were obtained for $\mu=0.3558$ and $\nu=0.2438$.

$\phi=0.5$, whereas $\mu+\nu$ determines the shape of the curve $k_{11}^{rel}=k_{11}^{rel}(\phi)$. For example, the height of the maximum at $\phi=0.5$ and the width of the curve described for group V (see Fig. 4) are independently controlled by $\mu-\nu$ and $\mu+\nu$, respectively.

Both μ and ν were determined by fitting $k_{11}^{rel}(\phi)$ only for group V. The best fit is obtained for $\mu=0.3558\pm0.0157$ and $\nu=0.2438\pm0.0210$. Then, these values are kept fixed for the other groups. The obtained theoretical curves (solid lines) are shown together with the simulated data (square symbols) in Fig. 7. As can be seen, the kinetic model reproduces the simulation results very satisfactorily for all groups and for all degrees of surface coverage.

Figure 8 depicts functions $f(\phi)$ (solid line) and ϕ (dashed line). As observed, $f(\phi)\geqslant\phi$ for all ϕ values. Since ϕ represents the probability for finding a surface patch at the first collision and $f(\phi)$ is the same probability after a given collision on the covered part of the particle, this result proves that the subsequent collisions have a higher probability to occur at the same configuration than the previous one.

It should be remembered that our simulations were performed without considering the particle rotational Brownian motion. This may lead to an overestimation of $f(\phi)$, since the correlation between the orientations of the particles at a first collision with the orientations of the consecutive ones would, in principle, decrease. Nevertheless, we expect only a slight change of $f(\phi)$ due to the rotational contribution.

Since the six groups of simulations were restricted to the particular cases (3) and (4), it would also be desirable to compare the simulation results with the theoretical predictions given by the general expressions (25) and (26), where the α values are not necessarily fixed to 0 or 1. Hence, a total number of 18 simulations were performed for different nontrivial values of α_1, α_2, and α_3 and taking $\phi=0.3$,0.5, and 0.8 (see Table II). Again, the theoretically obtained k_{11}^{rel} values match the simulated data quite satisfactorily. Note that for all cases, the relative error is lower than 2%.

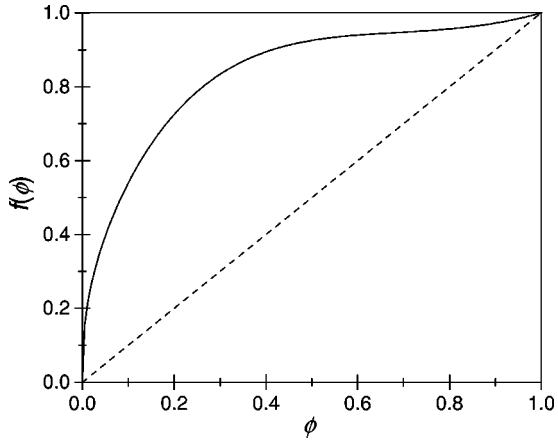

FIG. 8. $f(\phi)$ (solid line) and ϕ (dashed line) plotted as a function of ϕ. The fact that $f(\phi)\geqslant\phi$ means that subsequent collisions have a higher probability to occur in the same configuration as the previous one.

TABLE II. Comparison between the theoretical and simulated rate constants for different sets of sticking probabilities.

α			$\phi=0.3$		$\phi=0.5$		$\phi=0.8$	
α_1	α_2	α_3	$k_{11}^{rel}\|_{sm}$	$k_{11}^{rel}\|_{th}$	$k_{11}^{rel}\|_{sm}$	$k_{11}^{rel}\|_{th}$	$k_{11}^{rel}\|_{sm}$	$k_{11}^{rel}\|_{th}$
0.05	0.2	0.8	0.497	0.488	0.646	0.644	0.859	0.867
0.1	0.05	0.05	0.328	0.334	0.283	0.288	0.250	0.250
0.3	0.7	0.05	0.794	0.808	0.771	0.771	0.584	0.575
0.5	0.1	0.3	0.695	0.707	0.633	0.635	0.656	0.661
0.6	0.3	0.9	0.841	0.849	0.857	0.848	0.912	0.918
0.8	0.7	0.2	0.926	0.928	0.866	0.875	0.743	0.747

Finally, some curves calculated by using general expression (25) are shown for several values of the sticking probabilities in Fig. 9.

Since the geometrical probabilities P_{mn} and the sticking probabilities α_n are totally independent, the constant parameters μ and ν do not change with α_n. However, μ and ν characterize the geometrical aspects of the particle collisions and, therefore, they depend on the distribution of the surface coverage. Indeed, the values $\mu=\mu_0\equiv 0.3558$ and $\nu=\nu_0 \equiv 0.2438$ correspond to simulations performed by assuming a spotlike surface coverage. In contrast, for a homogeneously distributed surface coverage, the shorttime kinetics is described by the classical RLCA regime [Eq. (8)] and, consequently, the geometrical probabilities are not conditionalized to the previous collision: $P_{mn}=P_{0n}$. Comparing expressions (12) and (32) we obtain $\mu=1$ and $\nu=0$ for this particular case. When the coverage is distributed forming a given number of patches, values ranging in the intervals $\mu=[\mu_0,1]$ and $\nu=[0,\nu_0]$ are expected. Moreover, μ is an increasing function of the homogeneity of the spot spreading, whereas ν is a decreasing one. Consequently, μ and ν characterize the superficial homogeneity.

The previous model may, hypothetically, be extended for describing the moderate and long aggregation stages. This may be formally achieved by considering a size-dependent free surface coverage ϕ_i and by replacing $P_c \rightarrow (P_c)_{ij}$. However, this would be a very difficult, if not impossible, task by the following reasons. First, it is not clear whether the conditional geometrical probabilities P_{nm} could be written in terms of a single function $f(\phi)$. Second, and assuming that this single function exists, it would depend on the cluster size and on the way that particles associate (a dimer that is formed by bounding the covered patches of its constituting particles would show a small free degree of coverage, indeed). This clearly indicates that the aggregation regime will also affect the spot distribution on the free clusters surface, and hence, function f will also depend on the sticking probabilities α_n: $f=f_i(\phi_i,\alpha_1,\alpha_2,\alpha_3)$.

V. CONCLUSIONS

A model for describing the initial stages of the aggregation of spherical partially covered particles has been proposed. The motivation for this study is founded on the lack of an acceptable kinetic model for this kind of aggregating system. In fact, two previously proposed models were compared with the data obtained by means of computer simulations. In both cases, the results showed a clear mismatch between theory and simulation.

The model is based on the calculation of the average monomer lifetime, which is a function of the fraction of surface coverage, the sticking probabilities for each type of possible contacts, and the conditional geometrical probabilities for a given type of contact. This concepts lead to the definition of a function that quantifies the probability for two colliding particles to collide again on the same surface patch of one of the involved particles after a noneffective collision of any type. This function of the degree of surface coverage was then determined by computer simulations.

Unlike the initially tested models, the proposed model

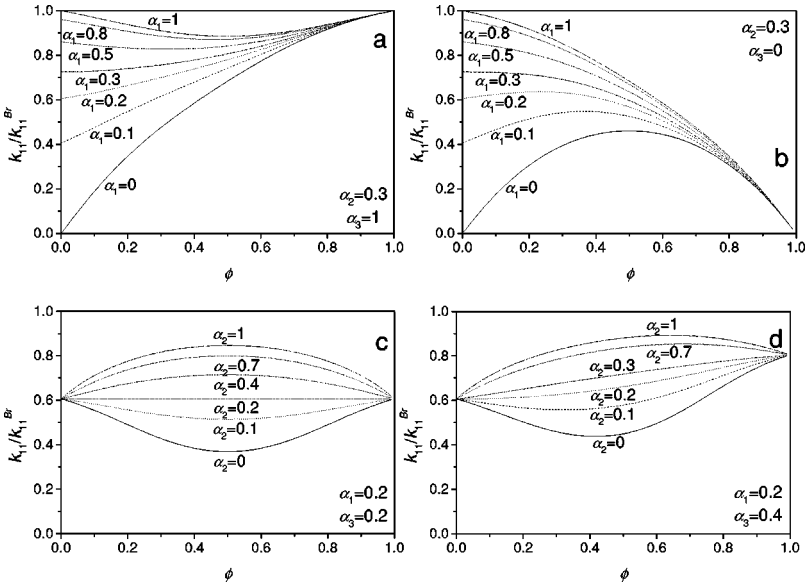

FIG. 9. Some curves calculated using general expression (25) are shown for the following sets of fixed sticking probabilities: (a) $\alpha_2=0.3$ and $\alpha_3=1$, (b) $\alpha_2=0.3$ and $\alpha_3=0$, (c) $\alpha_1=0.2$, and $\alpha_3=0.2$, and (d) $\alpha_1=0.2$ and $\alpha_3=0.4$.

leads to an accurate description of the initial kinetics for colloidal systems formed by partially covered spherical particles. This clearly demonstrates the importance of considering conditional geometrical probabilities for a correct description of the different encounters taking place in these kinds of aggregation processes.

ACKNOWLEDGMENTS

This work was supported by the Ministerio de Ciencia y Tecnología, Plan Nacional de Investigación, Desarrollo e Innovación Tecnológica (I+D+I) (Project Nos. MAT2000-1550-C03-01 and MAT2000-1550-C03-03).

[1] B.M. Moudgil and S. Behl, in *Flotation Science and Engineering*, edited by K.A. Matis (Marcel Dekker, New York, 1995).
[2] E. Dickinson and L. Eriksson, Adv. Colloid Interface Sci. **34**, 1 (1991).
[3] Y. Adachi, Adv. Colloid Interface Sci. **56**, 1 (1995).
[4] D. Napper, J. Colloid Interface Sci. **58**, 390 (1977).
[5] D. Napper, *Polymeric Stabilization of Colloidal Dispersions* (Academic Press, London, 1983).
[6] F. Fleer and J. Lyklema, J. Colloid Interface Sci. **52**, 228 (1974).
[7] J. Gregory, in *Solid-Liquid Dispersions*, edited by T.F. Tadros (Academic Press, London, 1987).
[8] V.K. La Mer and T.W. Healy, Rev. Pure Appl. Chem. **13**, 112 (1963).
[9] J.A. de Witt and T.G.M. van de Ven, Adv. Colloid Interface Sci. **42**, 41 (1992).
[10] J. Blaakmeer, M.R. Bohmer, M.A. Cohen Stuart, and G.J. Fleer, Macromolecules **23**, 2301 (1990).
[11] J.M. Peula and F.J. de las Nieves, Colloids Surf., A **90**, 55 (1994).
[12] T.G.M. van de Ven and B. Alince, J. Colloid Interface Sci. **181**, 73 (1996).
[13] M. Tirado-Miranda, A. Schmitt, J. Callejas-Fernández, and A. Fernández-Barbero, Langmuir **15**, 3437 (1999).
[14] M. Tirado-Miranda, A. Schmitt, J. Callejas-Fernández, and A. Fernández-Barbero, Langmuir **16**, 7541 (2000).
[15] Y. Adachi and T. Wada, J. Colloid Interface Sci. **229**, 148 (2000).
[16] T.H. Young, C.Y. Kao, Y. Hsieh, B.J. Wang, and J.P. Hsu, J. Colloid Interface Sci. **239**, 563 (2001).
[17] R.J. Owen, J.C. Crocker, R. Verma, and A.G. Yodh, Phys. Rev. E **64**, 011401 (2001).
[18] A. Thill, S. Moustier, J. Aziz, M.R. Wiesner, and J.Y. Bottero, J. Colloid Interface Sci. **243**, 171 (2001).
[19] G. Odriozola, A. Moncho-Jordá, A. Schmitt, J. Callejas-Fernández, R. Martínez-García, and R. Hidalgo-Álvarez, Europhys. Lett. **53**, 797 (2001).
[20] A. Moncho-Jordá, G. Odriozola, F. Martínez-López, A. Schmitt, and R. Hidalgo-Álvarez, Eur. Phys. J. E **5**, 471 (2001).
[21] M. von Smoluchowski, Phys. Z. **17**, 557 (1916).
[22] M. von Smoluchowski, Z. Phys. Chem., Stoechiom. Verwandtschaftsl. **92**, 129 (1917).
[23] A. Marmur, J. Colloid Interface Sci. **72**, 41 (1979).
[24] W.D. Brown and R.C. Ball, J. Phys. A **18**, L517 (1985).
[25] S.G. Ash and E.J. Clayfield, J. Colloid Interface Sci. **55**, 645 (1976).
[26] R. Hogg, J. Colloid Interface Sci. **102**, 232 (1984).
[27] B.M. Moudgil, B.D. Shah, and H.S. Soto, J. Colloid Interface Sci. **119**, 466 (1987).
[28] A. Molski, Colloid Polym. Sci. **267**, 371 (1989).
[29] P. Meakin, T. Vicsek, and F. Family, Phys. Rev. Lett. **31**, 564 (1985).
[30] A.E. González, Phys. Rev. Lett. **71**, 2248 (1993).
[31] R.L. Drake, in *Topic in Current Aerosol Research*, edited by G.M. Hidy and J.R. Brock (Pergamon Press, New York, 1972), Vol. 3.